ORIGINAL PAPER

Stationary and non-stationary temperature-duration-frequency curves for Australia

Orpita U. Laz[1] · Ataur Rahman[1] · Taha B. M. J. Ouarda[2] · Nasreen Jahan[3]

Abstract

Australian summer heat events have become more frequent and severe in recent times. Temperature-duration-frequency (TDF) curves connect the severity of heat episodes of various durations to their frequencies and thus can be an effective tool for analysing the heat extremes. This study examines Australian heat events using data from 82 meteorological stations. TDF curves have been developed under stationary and non-stationary conditions. Generalised Extreme Value (GEV) distribution is considered to estimate extreme temperatures for return periods of 2, 5, 10, 25, 50 and 100 years. Three major climate drivers for Australia have been considered as potential covariates along with *Time* to develop the non-stationary TDF curves. According to the Akaike information criterion, the non-stationary framework for TDF modelling provides a better fit to the data than its stationary equivalent. The findings can be beneficial in offering new information to aid climate adaptation and mitigation at the regional level in Australia.

Keywords Annual maximum temperature · Climate change · Climate drivers · Generalised extreme value · Non-stationary · Temperature-duration-frequency

1 Introduction

Intergovernmental Panel on Climate Change (IPCC) estimated that the mean global temperature would exceed the higher limit of increase in temperature adopted in the Paris agreement by the 2040s (IPCC 2018). It was also reported

✉ Ataur Rahman
  a.rahman@westernsydney.edu.au

  Orpita U. Laz
  183171116@student.westernsydney.edu.au;
  orpita12@yahoo.com

  Taha B. M. J. Ouarda
  Taha.Ouarda@inrs.ca

  Nasreen Jahan
  nasreenjahan@wre.buet.ac.bd

[1] School of Engineering, Design and Built Environment, Western Sydney University, Locked Bag 1797, Penrith, NSW 2751, Australia

[2] Canada Research Chair in Statistical Hydro-Climatology, Institut national de la recherche scientifique INRS-ETE, Quebec City, Canada

[3] Department of Water Resources Engineering, Bangladesh University of Engineering and Technology, Dhaka, Bangladesh

in 2020 that the temperature in Australia has increased by 1.44 ± 0.24 °C since 1910 (CSIRO and Australian Government (Bureau of Meteorology) 2020). Generally, changes in maximum and minimum temperatures impact the environment more than mean temperature (Sein et al. 2018) and adversely influence the events related to extreme temperature (Chowdary et al. 2014). Extreme temperature triggers more natural hazards, i.e. droughts, bushfires, heatwaves, cyclones, and negatively affects human health, agriculture, ecosystems and infrastructure (Omer et al. 2020; Suman and Maity 2020). Therefore, predicting extreme temperatures for a particular duration and return period is important in many aspects of our lives. Some are relevant to health, energy and agriculture, urban planning, and ecology management. In this context, the design temperatures for the selected durations and return periods can be estimated following the same principle of rainfall Intensity–Duration–Frequency (IDF) curves, which have been utilised for many years for the design and management of hydrological infrastructure as well as flood risk management (Yan et al. 2019). Extreme value theory has been accepted globally to construct IDF curves by fitting theoretical probability distribution functions to annual

maximum rainfall time series (Cheng and Aghakouchak 2014; Yan et al. 2020).

Most of the works found in the literature on IDF curves are based on the temporal stationarity concept (Singh and Zhang 2007; Jakob 2013), implying that the occurrence probability of precipitation events will not change significantly over time. However, in reality, the frequency, magnitude and duration of hydroclimatic extremes, i.e. extreme rainfall (Galiatsatou and Iliadis 2022), floods (Berghuijs et al. 2019), droughts (Spinoni et al. 2017), and heatwaves (Lorenz et al. 2019) fluctuates beyond the stationary envelope of variability. Furthermore, it is also observed that the IDF curve considering stationarity, often underestimates the return level of rainfall (Sugahara et al. 2009; Cheng and Aghakouchak 2014). Therefore, to increase the reliability of IDF curves, it is suggested to incorporate the non-stationarity of the distribution parameters in hydrological models (Sarhadi and Soulis 2017), especially at their extreme levels (Ganguli and Coulibaly 2017).

In the construction of IDF curves, covariates are generally introduced to apprehend the non-stationarities in time series. Any drivers that are correlated to the selected events can be considered as a candidate for such covariates (Katz et al. 2002; Hundecha et al. 2008), which can be low-frequency climatological signals (Coles 2001) as well as time (Sugahara et al. 2009; Yilmaz and Perera 2014). In this approach, the parameters of the Generalised Extreme Value (GEV) distribution are expressed as a linear or non-linear function of covariates (Kwon and Lall 2016; Sarhadi and Soulis 2017). This approach has been effectively employed in extreme rainfall events around the world (Ouarda et al. 2019), including Australia (Yilmaz and Perera 2014).

Although there have been extensive works carried out on the development of IDF curves all over the globe, very limited works are found in the literature on the construction of Temperature-Duration-Frequency (TDF) curves, which relate temperature intensities corresponding to varying durations and return periods (Wang et al. 2013; Ouarda and Charron 2018). Moreover, no TDF curves have been constructed for Australia till date.

In this study, time series data of the daily maximum temperature of Australia at selected stations are analysed, and the best climate-informed covariates are selected from the most influential covariates for the annual maximum temperature (AMT) to characterise the physical process related to the dynamics of the extreme temperature. For this purpose, three climate drivers (CDs), namely—El Niño Southern Oscillation (ENSO), Southern Annular Mode (SAM) and Indian Ocean Dipole (IOD), are selected along with the *Time* as potential covariates. After that, stationary TDF curves are constructed following the frequency

analysis method, already adopted in the construction of IDF curves, for different durations and return periods. The present work also extends these stationary TDF curves to non-stationary conditions according to the framework outlined by Ouarda and Charron (2018). Then, based on the Akaike Information Criterion (AIC) value, the best model for each selected station is identified, and the TDF curves are constructed under stationary and non-stationary conditions. Finally, the influence of non-stationarity on the TDF curves is assessed.

2 Study area and data

The whole Australia is considered as the study area except Tasmania (Fig. 1). Australia experiences a variety of climates across the country because of a wide range of geographical extent consisting of tropical-influenced climate in the northern and north-eastern zones, Mediterranean-like climate in the southern coastal zones and desert climate in most of the central interior zones (Turney et al. 2007).

2.1 Temperature time series

All the recorded daily maximum temperatures across Australian weather stations were examined for inconsistency, outliers and gaps. The stations, which had less than 5% missing data over the last five decades covering the time period from 1969 to 2021, were selected for analysis. According to the above mentioned criterion, 82 weather stations in Australia (out of 1415 weather stations) were initially selected as candidate stations. The gaps in the daily maximum temperature time series in the initially
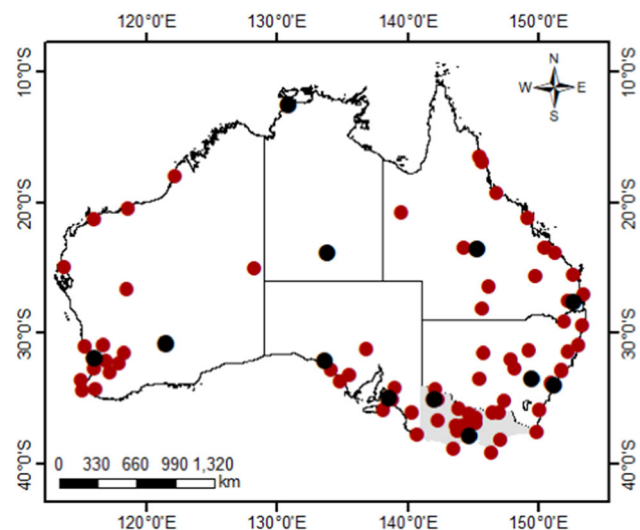
Fig. 1 Study area and selected stations (stations marked with black circles are described in detail in this paper)

selected stations were spatially interpolated with the same time series data from surrounding weather stations located within a 30 km radius. The locations of the initially selected temperature stations are shown in Fig. 1. For the subsequent analysis, a total of 12 stations were selected, two from each of the six Australian states (New South Wales, Queensland, The Northern Territory, Western Australia, South Australia and Victoria) as shown in Fig. 1.

The annual maximum daily temperatures were calculated for each selected weather station from the recorded daily maximum temperature data. Particular attention was given to the summer season of Australia, which is considered to be December to February, and the extended summer is considered to be from November to March. Therefore, the annual maximum daily temperature calculated from each calendar year would have been divided into summer or extended summer seasons into two consecutive years. Therefore, the hydrological year in Australia, starting from April to March, instead of the calendar year, was considered in this study to calculate the annual maximum daily temperature.

2.2 Covariates

Australia is extremely susceptible to changes in the ocean–atmosphere system. The inter-annual dynamics of Australia's seasonal weather are regulated by the climatic variability of three neighbouring oceans—the Pacific, Indian, and Southern Oceans (Cai et al. 2014; Maher and Sherwood 2014; Oliveira and Ambrizzi 2017), known as CDs. Three primary CDs strongly influence Hydroclimate in Australia—The El Niño Southern Oscillation (ENSO) (Power et al. 1999; Cai and Van Rensch 2012), Southern Annular Mode (SAM) (Thompson et al. 2000; Risbey et al. 2009) and Indian Ocean Dipole (IOD) (Ummenhofer et al. 2009; Ummenhofer et al. 2011).

Therefore, in this study, three physical processes, in which two of them from the sea surface temperature—ENSO, IOD and one from air pressure—SAM, and also *Time,* were considered to be one of the potential covariates to identify the best covariate for developing non-stationary TDF curves.

2.2.1 El Niño-Southern Oscillation (ENSO) cycle

The El Nino-Southern Oscillation (ENSO) is considered to be a major CD over many regions of the globe (Ropelewski and Halpert 1988; Halpert and Ropelewski 1992), including Australia (Nicholls 1985). The SST index is considered the monthly sea surface temperature anomaly over NINO3.4 (17°E–120°W, 5°S–5°N) region (Bellenger et al. 2014) and was used as a covariate representing ENSO. Nino3.4 was obtained from https://psl.noaa.gov/gcos_wgsp/Timeseries/Nino34.

ENSO is considered to be a strong CD in Australia (Power et al. 2006; Risbey et al. 2009; Arblaster and Alexander 2012), especially in southeastern Australia (Nicholls and Lucas 2007) and northeast Australia (Min et al. 2013; Cowan et al. 2014; Perkins et al. 2015), but weak in the far southeast of Australia (Parker et al. 2013; Boschat et al. 2015). In Australia, it has been observed that the strength of ENSO decreases along a north–south gradient.

2.2.2 Indian Ocean Dipole (IOD)

The Indian Ocean Dipole (IOD) is represented with Dipole Mode Index (DMI) (Saji et al. 1999; Meyers et al. 2007; Liu et al. 2014) and calculated as the difference of SST anomalies in the western equatorial Indian Ocean (50 to 70°E, 10°S to 10°N) minus those in the east (90 to 110°E, 10°S to 0° N). The monthly DMI was derived from https://psl.noaa.gov/gcos_wgsp/Timeseries/DMI/ and considered as a covariate that represents IOD.

IOD has been identified as the major driver for Eastern Australia (Meyers et al. 2007; Risbey et al. 2009; Cai et al. 2011) and has a positive correlation with maximum temperatures during winter and spring (May and November) (Min et al. 2013; White et al. 2013).

2.2.3 SAM

The Southern Annular Mode (SAM) describes the north–south movement of the westerly wind belt that circles Antarctica and is a monthly mean sea level pressure (MSLP) anomaly time dataset. The data for this index were obtained from http://www.nerc-bas.ac.uk/icd/gjma/sam.html.

SAM considerably impacts the rainfall in Australia (Hendon et al. 2007), particularly in southern Australia. SAM is even associated with 10–15% of the rainfall in southwest Australia. SAM also affects the temperature in Australia and is identified as the main CD for the southwestern land division in western Australia (Guthrie 2021).

2.2.4 Time

Time has been utilised as a covariate to investigate the non-stationarity in the IDF curves all over the world (Sugahara et al. 2009; Yilmaz and Perera 2014). Therefore, in this study, *Time* was also considered as one of the potential covariates to construct the non-stationary TDF curves. The hydrological years of the AMT series were transformed into a series of integers from 1 to the number of years of the selected time duration and considered as a covariate representing *Time*.

3 Methodology

In this study, firstly, the non-stationarity of the temperature data series was assessed to justify the requirements of the incorporation of the non-stationarity in the construction of TDF curves. Then, the correlations between the selected three physical processes—ENSO, SAM and IOD were computed to identify the best covariate. In this approach, *Time* was also used as one of the covariates. Different non-stationary models were constructed considering different covariates stated earlier as well as their combination. Finally, *Time* or any of the selected physical processes (ENSO, IOD and SAM) was considered a covariate in models with one covariate.

Similarly, *Time* and one climate index (*Time*—ENSO, *Time*—IOD and *Time*—SAM) were adopted in models with two covariates. First, the best model for the AMT series was chosen based on the Akaike information criterion (AIC). After identifying the best non-stationary model, the non-stationary design temperature was computed using the parameters of the best non-stationary model.

GEV distribution was selected to develop both stationary and non-stationary TDF curves as it is widely used to model climatic extremes (Ouarda and Charron 2018; Ouarda et al. 2020; Haddad 2021; Devi et al. 2022). Under the condition of stationary, three parameters of the GEV distributions, μ, σ, ξ, which are the location, scale and shape parameters, respectively, were assumed to be constant, whereas, under non-stationary conditions, the parameters were expressed as a linear or quadratic function of the covariate(s). However, the shape parameter was assumed to be constant for all the cases since the reliability of modelling the shape parameter is low (Cheng et al. 2014; Ganguli and Coulibaly 2017). The distribution parameters were calculated using the maximum composite likelihood method utilising the optimisation function *fmincon* in MATLAB. Finally, the stationary and non-stationary TDF curves were compared to assess the influence of non-stationarity in the construction of TDF curves.

3.1 Detection of non-stationarity in temperature time series

All the historical records of AMT at the selected stations over the selected time period were tested for non-stationary signals. An augmented Dickey-Fuller (ADF) test was applied to the AMT data series for each of the selected stations. In this test, the null hypothesis assumes that the data series is non-stationary and thereby considered stationary when the null hypothesis is rejected at the selected significance level.

3.2 Correlation between climate drivers (CDs) and temperature time series

The relations between the AMT for all the selected stations and CDs—ENSO, SAM and IOD were tested using correlation analyses considering both concurrent and time-lagged relationships.

The covariates representing CDs in this study were computed as the moving averages of corresponding CDs over three consecutive months starting from April and ending in March of the next year, covering the full hydrological year and denoted in this study by the first letter of the three months (AMJ, MJJ, JJA, JAS, ASO, SON, OND, NDJ, DJF, JFM). To determine the appropriate season of the CD acting as the predictor of the AMT, correlations between seasonal CDs and AMTs were explored. Best covariates and the suitable season were selected based on the higher correlation values between the AMT series and CDs averaged over the selected season. This selection process was also validated graphically by plotting all the correlations between the AMT time series and all the CDs for all seasons.

3.3 Construction of TDF curves

(i)   General TDF relationship

The general TDF relationship can be expressed by following the formulation for IDF curves proposed by Rossi and Villani (1994) and Koutsoyiannis et al. (1998):

$$t_R(d) = \frac{a(R)}{b(d)} \qquad (1)$$

where d is the duration and R is the return period. In this formulation, the dependency of return level, $t_R(d)$ on R and d can be modelled separately. The distribution of maximum average temperature $T(d)$ governs the function $a(R)$ that defines the TDF curves, which remain parallel for various return periods. The function $b(d)$ controls the shape of the TDF curves and is given as:

$$b(d) = (d + \theta)^\eta \qquad (2)$$

where θ and η are the shape parameters subjected to the boundary conditions of $\theta > 0$ and $0 < \eta < 1$.

If the probability distribution of $T(d)$ is denoted by $F_{T(d)}(t; d)$, where t indicates the maximum average temperature and d represents the durations, $Y = T(d)b(d)$, which is the scaled maximum average temperature distributed as $F_{T(d)}(t; d)$ (i.e., $F_{T(d)}(t; d) = F_Y(y_R) = 1 - \frac{1}{R}$). Consequently, the expression $a(R)$ is given by:

$$a(R) = F_y^{-1}\left(1 - \frac{1}{R}\right) \qquad (3)$$

(ii)   Stationary TDF curves

The GEV distribution is the most widely used probability distribution that is used to model climate extremes, and hence, the GEV distribution is used here to model $T(d)$. The cumulative distribution function of the GEV is given by:

$$F(x) = \exp\left\{-\left[1 + \kappa\left(\frac{x-\mu}{\sigma}\right)\right]^{-1/k}\right\}, \quad (4)$$

where μ, σ and κ are the location, scale, and shape parameters, respectively. $F(x)$ is defined for $1 + \frac{\kappa(x-\mu)}{\sigma} > 0$, where $\sigma > 0$.

The general stationary TDF relationship based on the GEV distribution can be expressed as (Ouarda and Charron 2018):

$$t_R(d) = \frac{a(R)}{b(d)} = \frac{\mu - \frac{\sigma}{\kappa}\left\{1 - \left[\log\left(1 - \frac{1}{R}\right)^{-\kappa}\right]\right\}}{(d+\theta)^\eta} \quad (5)$$

(iii)   Non-stationary TDF curves

To incorporate non-stationarity in Eq. (5), the three parameters of the GEV distribution described in Eq. (4) are considered to be dependent on time to incorporate the non-stationarity in TDF curve development and Eq. (4) can be expressed as:

$$F(x) = \exp\left\{-\left[1 + \kappa(t)\left(\frac{x-\mu(t)}{\sigma(t)}\right)\right]^{-1/k}\right\}, \text{ for } 1$$
$$+ \frac{\kappa(t)(x-\mu(t))}{\sigma(t)} > 0 \quad (6)$$

In this exploratory study, the location and scale parameters are considered to vary with covariates linearly or quadratically, while all other shape parameters, θ, η and κ for the GEV distribution are assumed to be constant (Katz et al. 2002; Adlouni and Ouarda 2009).

The vectors of the distribution parameters $\psi = (\mu, \sigma, \theta, \eta)$ and $\psi = (\mu_0, \mu_1, \ldots, \sigma_0, \sigma_1, \ldots, \kappa, \theta, \eta)$ are estimated using the maximum composite likelihood for stationary and non-stationary TDF curves, respectively.

4 Results and discussion

The results for 12 stations (two stations from each state in Australia and shown as black dots in Fig. 1) are presented in greater detail (out of the 82 selected stations) in the following sections.

4.1 Detection of non-stationarity

The augmented Dickey-Fuller (ADF) test was applied to each AMT data series (covering 1969–2021) separately for

Table 1 Summary of ADF test statistics and p-values for selected 12 stations in Australia

Station ID	Station	*p*-value	Test statistics
066037	Sydney airport AMO	0.465	− 2.252
063005	Bathurst agricultural station	0.088	− 3.246
014015	Darwin airport	0.052	− 3.493
015590	**Alice springs airport**	**0.008**	**− 4.244**
009021	**Perth airport**	**0.004**	**− 4.579**
012038	Kalgoorlie-boulder airport	0.050	− 3.506
040004	**Amberley AMO**	**0.006**	**− 4.364**
036007	**Barcaldine post office**	**0.047**	**− 3.532**
018012	Ceduna AMO	0.454	− 2.275
023034	Adelaide airport	0.060	− 3.424
087031	Laverton RAAF	0.194	− 2.829
076064	Walpeup research	0.121	− 3.088

Bold font indicates a p-value smaller than 0.05

each selected station. Based on the ADF tests, the test statistics and p-value for 12 stations are summarised in Table 1. Four stations showed ADF test statistics below the critical value (− 3.507), and the p-values were less than 0.05 at the 95% confidence level, as shown in boldface in Table 1. For these stations, the null hypothesis was rejected, and the data series was considered stationary. Therefore, the null hypothesis could not be rejected for the rest of the stations, and the non-stationarities in the data series were detected. Although all the available stationarity tests have some drawbacks and are not decisive alone (Cai et al. 2009a, b), the results of ADF tests here highlighted the presence of the non-stationarity in the AMT time series and consequently emphasised the importance of incorporating the non-stationarity in the construction of TDF curves.

4.2 Correlation analysis and covariate selection

The correlations between the AMT and the ENSO, IOD and SAM for all the seasons are presented in Supplementary Section (Figures S1, S2 and S3).

The correlations between ENSO and the AMT were the strongest and statistically significant during the spring and summer seasons, particularly in the eastern regions of Australia. The positive influence of the ENSO on the temperature was weaker at the beginning of the hydrological year and increased gradually over the year. At the end of the hydrological year, this influence became weak, even negative for some stations.

Similar to the ENSO, positive influences of IOD on the temperatures were also identified all over Australia. This influence was enhanced during the spring season and was statistically significant in the southeastern region of

Australia. However, at the end of the hydrological year, the impact of IOD also became weaker and negative at some stations.

Considering the correlation values between the CDs averaged over different seasons and the temperature, one CD was selected for each station along with the occurring season, as shown in Fig. 2.

One of the main findings of this study was that ENSO in spring acted as the dominant CD for the stations located in the inland NSW, Queensland and Western Australia, which is similar to the findings by a few other researchers (Min et al. 2013). On the other hand, IOD had the strongest relations with temperature along the east coast and almost all stations in the coastal and inland regions of Victoria and South Australia. It should be noted that there is a significant decrease in rainfall across southern Australia as the frequency of positive IOD events has increased, which contributed to significant bushfires over southeastern regions of the continent (Cai, Cowan and Raupach, 2009; Cai et al. 2009a, b).

Although SAM in Autumn had strong relations with stations in NSW and Victoria, ENSO and IOD were the dominant CDs. Furthermore, one of the Department of Primary Industries and Regional Development studies reported a decline in rainfall due to SAM in southern Australia, particularly in the southwest region (Guthrie 2021). However, SAM appeared as the selected CD at the stations located in the coastal regions of Western Australia. In the cases of stations located in the Northern Territory, the temperature recorded at the station on the coastal side was associated with ENSO, while at the inland, it was correlated with the IOD.

The Pearson correlation coefficient values for the AMT series from April–May–June (AMJ) to January–February–March (JFM) of the same hydrological year recorded at 12 stations are presented in Fig. 3. These illustrations validated the selection of the best CDs and seasons presented
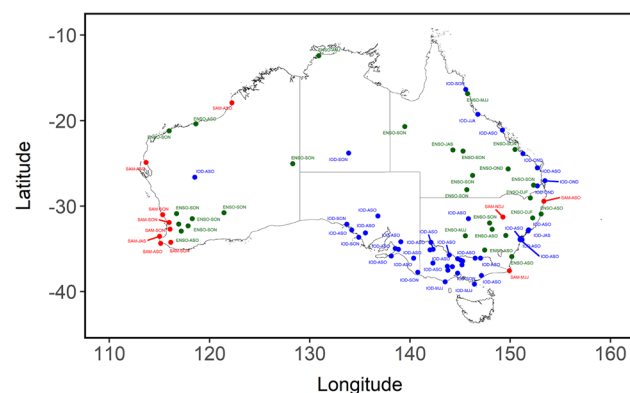
in Fig. 2. Selected CDs with the seasons for the selected 12 stations are summarised in Table 2.

4.3 Stationary TDF

Figure 4 illustrates the stationary TDF curves based on GEV distribution as described in the methodology section. Estimated temperatures were plotted against the selected durations (1, 2, 3, 4, 5, 6, 7 and 10 days), with each curve indicating a different return period such as 2, 5, 10, 25, 50 and 100 years at stationary scale. These TDF curves demonstrated a significant rise in temperature with higher return periods and decreased with the increase in duration for all the selected stations.

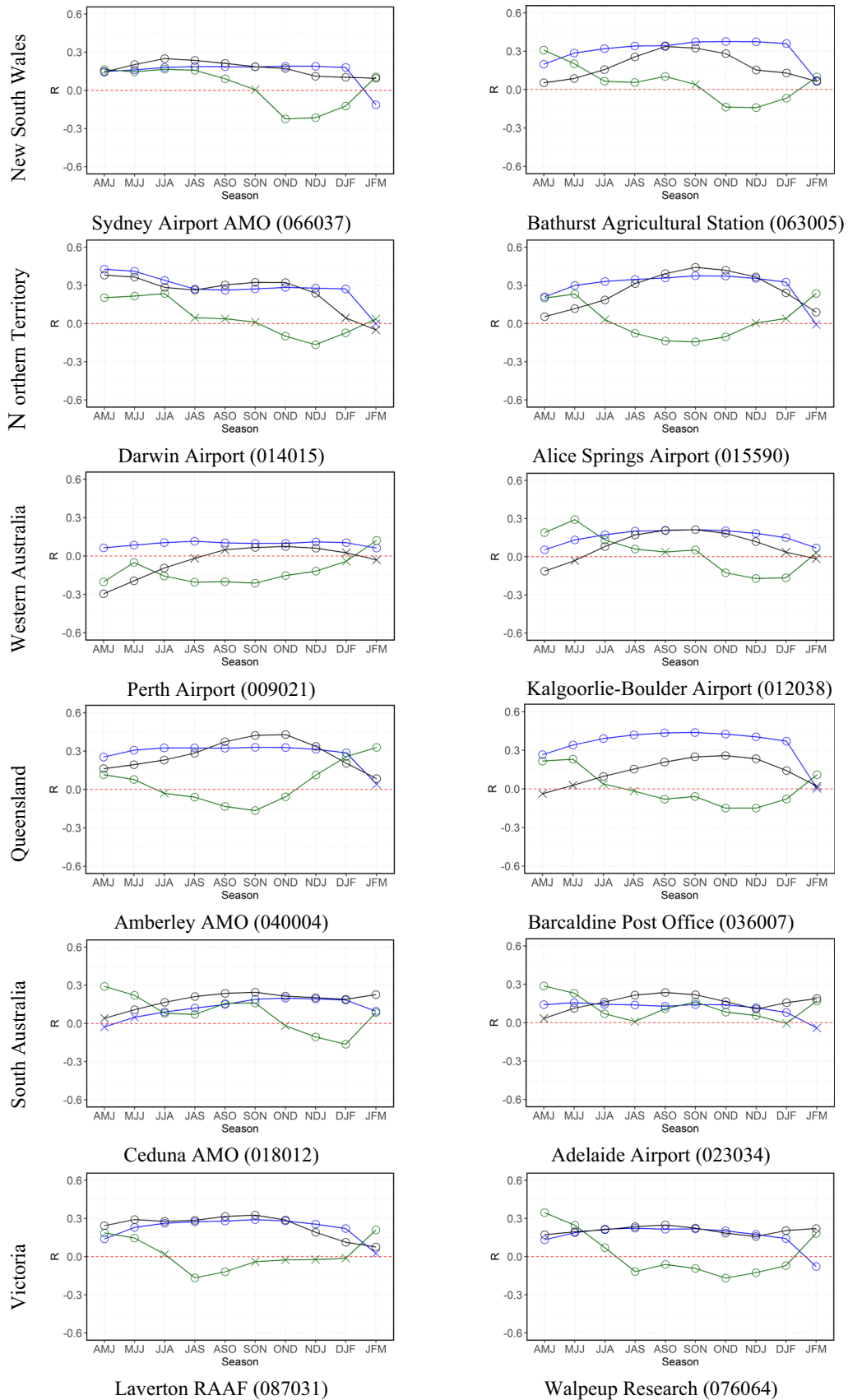### 4.4 Non-stationary TDF surfaces

For each TDF model and station, the maximal independence log-likelihood, the CL-AIC statistic, and the model parameters are summarised in Table 3. According to the values obtained by the AIC criterion from each model, the table only shows the optimal parameter relationship among the constant, linear and quadratic relationships to the covariate or the combinations of the covariates.

The CL-AIC statistic and log-likelihood suggested that the *Time* and covariate individually or combinedly increased the goodness-of-fit compared to the stationary model for all the stations. It's worth noting that employing a non-stationary model or the GEV enhances the log-likelihood in every case. However, the performances of different stationary and non-stationary TDF models were compared by the CL-AIC values, which were penalised due to the inclusion of more variables and thereby provided more reliable results.

Most stations (9 out of 12) with a combination of *Time* and CD as covariates showed the best goodness-of-fit. This suggested that the combination of the two covariates considerably impacted severe temperatures. *Time* was more prominent than CDs and qualified as the best covariate in cases of Sydney Airport AMO and Laverton RAAF stations. On the other hand, for Barcaldine Post Office, the influence of covariate alone was stronger than *Time* or the combination of *Time* and CD as the covariate.

4.4.1 Non-stationary TDF surfaces—One covariate (Time or CD)

Figures 5 and 6 present the non-stationary TDF graphs with the model considering *Time* and CD as a covariate for the typical stations. For all the illustrated stations in this study, non-stationary TDF models with *Time* as a covariate, either scale or location parameters were found to be varied linearly with time, except for Darwin, Alice Springs

Fig. 2 Selected climate drivers (CDs) with season based on the correlations between AMT and the CDs (ENSO, IOD and SAM) during 1969–2021

Sydney Airport AMO (066037)

Bathurst Agricultural Station (063005)

Darwin Airport (014015)

Alice Springs Airport (015590)

Perth Airport (009021)

Kalgoorlie-Boulder Airport (012038)

Amberley AMO (040004)

Barcaldine Post Office (036007)

Ceduna AMO (018012)

Adelaide Airport (023034)

Laverton RAAF (087031)

Walpeup Research (076064)

◄ **Fig. 3** Correlations between AMT and CDs. The blue, black and green lines represent correlations between AMT and ENSO, IOD and SAM, respectively

Airport, Adelaide Airport, Walpeup Research, where either of the parameters varied quadratically with time. TDF curves with *Time* as a covariate for Kalgoorlie-Boulder Airport stations linearly varied with time but were not parallel to each other for different return periods. It needs further investigation, which is left for future research. In the case of Perth stations, the estimated temperature increased with return periods and decreased with duration but did not vary significantly with time. However, in the case of non-stationary TDF models with CDs as covariates, the scale or location parameters varied quadratically with selected CDs for most stations.

Consequently, the TDF curves varied parabolically with CDs. Exceptions were observed for Sydney Airport AMO, Alice Spring Airport, Amberly AMO, Adelaide Airport and Walpeup Research stations, where either scale or the location parameter changed linearly with CDs and exhibited linear TDF curves for different return periods and durations. These characteristics of non-stationary TDF models can be seen distinctively in Figures S4—S7 (in supplementary sections).

4.4.2 Non-stationary TDF surfaces—Two covariates (*Time* and CDs as covariates)

For non-stationary TDF models incorporating two covariates, five variables are required to be present in the graph. Therefore, in this paper, non-stationary TDF surfaces are presented in two ways—either the duration is kept fixed and TDF surfaces for different return periods are presented, or return period is kept fixed and TDF surfaces for different durations are illustrated. Figure 7 shows the TDF surfaces

for 5-day duration and all the return periods considered in this study, whereas Fig. 8 presents the TDF surfaces for 50-year return period and all the considered durations.

4.5 Impacts of non-stationarity on TDF curves

The temperature quantiles calculated at a given time are significantly affected by incorporating one or more covariates. Figure 9 shows the graphs of the 50-year quantiles versus the duration for the stationary TDF model and the non-stationary TDF models considering different *Time* and covariates representing different scenarios for each station. The non-stationary quantiles for the first and last years of the study period were computed with *Time* covariate and denoted as *Time* (1970) and *Time* (2021) to display the quantiles' temporal movement. The years with the highest and lowest values of the selected seasonal CDs throughout the period 1970–2021 were selected for "CD" and "*Time* + CD" non-stationary models to highlight the influence of the extreme conditions on the estimated quantiles. All the graphs illustrated in Fig. 9 use the model that provides the greatest overall fit.

In all stations, it was observed that the influence of the duration on the difference in quantile estimation between the stationary and non-stationary models was negligible. For all the 12 stations, the stationary model always overestimated and underestimated the return levels in the case of the non-stationary models with the earliest (1970) and latest (2021) years of the study period as *Time* covariate, respectively. The stationary model overestimated upto 4.2 °C compared to the former cases, while underestimated upto 2.3 °C for the latter cases at all the12 stations. The only exception was for the Perth Airport station, where *Time* covariate had no significant influence. This can be explained by the fact that the Perth Airport station showed no non-stationarity (Table 1) and no temporal trend in the

Table 2 Pearson correlation coefficients between the AMT series and the selected seasonal climate index

Station ID	Station name	Latitude	Longitude	Climatic driver and season	Correlation coefficient value
066037	Sydney airport AMO	− 33.95	151.17	IOD(JJA)	0.25
063005	Bathurst agricultural	− 33.43	149.56	ENSO(SON)	0.37
014015	Darwin airport	− 12.42	130.89	ENSO(AMJ)	0.43
015590	Alice springs airport	− 23.80	133.89	IOD(SON)	0.38
009021	Perth airport	− 31.93	115.98	SAM(SON)	− 0.21
012038	Kalgoorlie-boulder airport	− 30.78	121.45	SAM(MJJ)	0.29
040004	Amberley AMO	− 27.63	152.71	IOD(OND)	0.43
036007	Barcaldine post office	− 23.55	145.29	ENSO(SON)	0.44
018012	Ceduna AMO	− 32.13	133.70	IOD(SON)	0.25
023034	Adelaide airport	− 34.95	138.52	IOD(ASO)	0.24
087031	Laverton RAAF	− 37.86	144.76	IOD(SON)	0.33
076064	Walpeup research	− 35.12	142.00	IOD(ASO)	0.25

Fig. 4 Stationary TDF curves for 2, 5, 10, 25, 50 and 100 years return periods
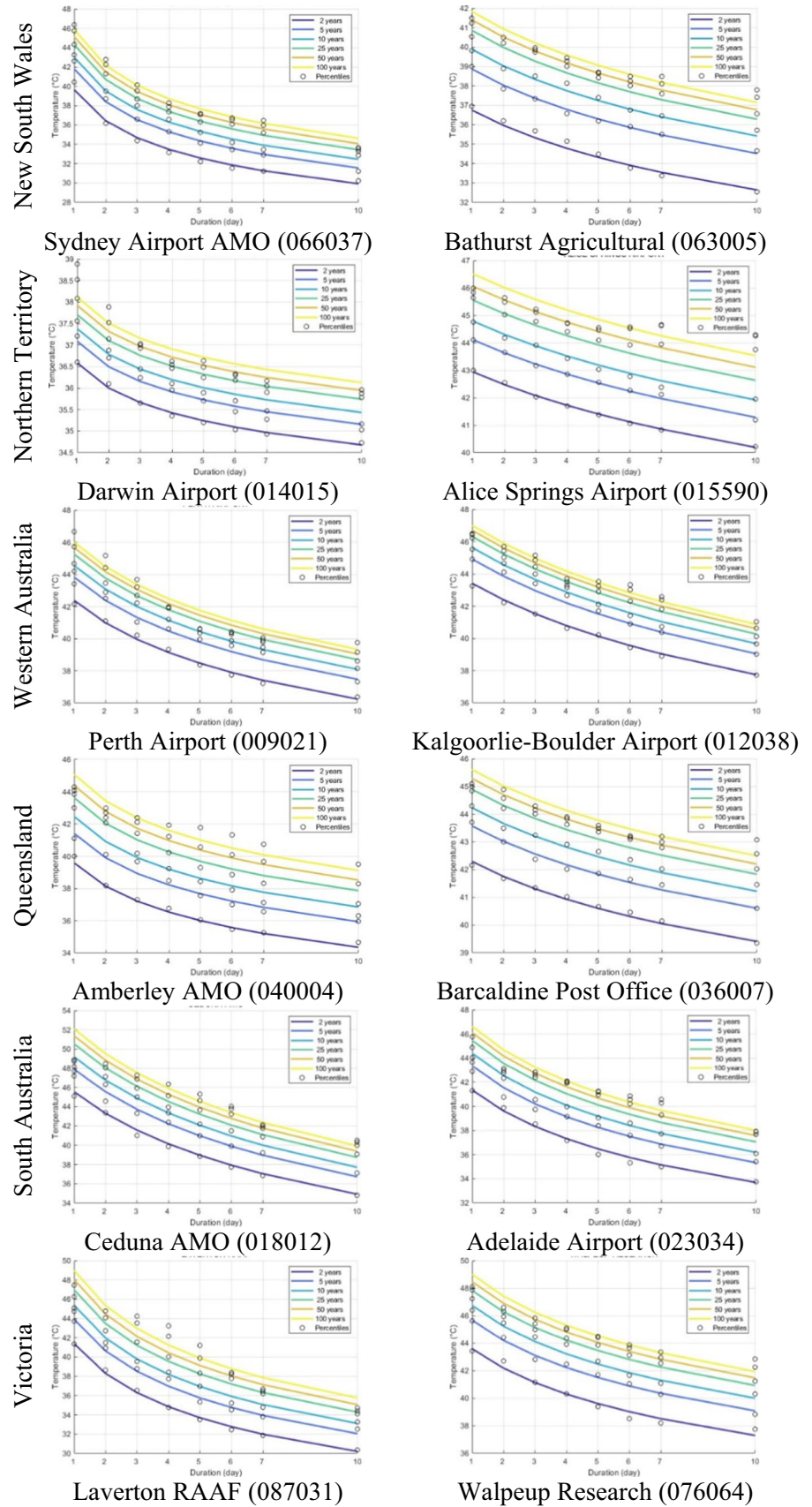
Table 3 Summary of parameters for the selected models and their error estimation

Station	Model	l_{ind}	CL-AIC	Model parameters
Sydney airport AMO	Stationary	− 881.47	1791.45	μ, σ
	Time	− 866.07	**1775.35**	$\mu_l = \mu_0 + \mu_1 T, \sigma$
	CD	− 873.53	1787.97	$\mu_l = \mu_0 + \mu_1 I, \sigma$
	Time + CD	− 863.46	1780.83	$\mu_l = \mu_0 + \mu_1 I + \mu_2 T, \sigma$
Bathurst agricultural station	Stationary	− 939.29	1917.13	μ, σ
	Time	− 851.05	1751.47	$\mu_l = \mu_0 + \mu_1 T, \sigma$
	CD	− 895.64	1854.87	$\mu_l = \mu_0 + \mu_1 E + \mu_2 E^2, \sigma$
	***Time* + CD**	− 808.35	**1692.00**	$\mu_l = \mu_0 + \mu_1 E + \mu_2 E^2 + \mu_3 T, \sigma$
Darwin airport	Stationary	− 324.62	676.26	μ, σ
	Time	− 262.29	572.28	$\mu_l = \mu_0 + \mu_1 T + \mu_2 T^2, \sigma$
	CD	− 287.11	625.63	$\mu_l = \mu_0 + \mu_1 E + \mu_2 E^2, \sigma$
	***Time* + CD**	− 234.22	**525.28**	$\mu_l = \mu_0 + \mu_1 E + \mu_2 T + \mu_3 T^2, \sigma$
Alice springs airport	Stationary	− 675.70	1390.62	μ, σ
	Time	− 642.08	1358.22	$\mu_l = \mu_0 + \mu_1 T$
				$\sigma_l = \sigma_0 + \sigma_1 T + \sigma_2 T^2$
	CD	− 623.41	1304.61	$\mu_l = \mu_0 + \mu_1 I$
				$\sigma_l = \sigma_0 + \sigma_1 I$
	***Time* + CD**	− 621.70	**1304.38**	$\mu_l = \mu_0 + \mu_1 I + \mu_2 T, \sigma$
Perth airport	Stationary	− 763.95	1557.98	μ, σ
	Time	− 763.95	1567.02	$\mu, \sigma_1 = \sigma_0 + \sigma_1 T$
	CD	− 736.19	1526.39	$\mu_l = \mu_0 + \mu_1 S + \mu_2 S^2$
				$\sigma_l = \sigma_0 + \sigma_1 S + \sigma_2 S^2$
	***Time* + CD**	− 732.25	**1524.26**	$\mu_l = \mu_0 + \mu_1 S + \mu_2 S^2 + \mu_3 T$
				$\sigma_l = \sigma_0 + \sigma_1 S + \sigma_2 T$
Kalgoorlie-boulder airport	Stationary	− 791.51	1616.49	μ, σ
	Time	− 774.88	1588.99	$\mu, \sigma_1 = \sigma_0 + \sigma_1 T$
	CD	− 764.00	1582.79	$\mu_l = \mu_0 + \mu_1 S + \mu_2 S^2, \sigma$
	***Time* + CD**	− 741.39	**1554.90**	$\mu_l = \mu_0 + \mu_1 S + \mu_2 S^2 + \mu_3 T$
				$\sigma_l = \sigma_0 + \sigma_1 S + \sigma_2 T$
Amberley AMO	Stationary	− 844.36	1728.03	μ, σ
	Time	− 798.10	1649.35	$\mu_l = \mu_0 + \mu_1 T, \sigma$
	CD	− 806.68	1665.05	$\mu_l = \mu_0 + \mu_1 I, \sigma$
	***Time* + CD**	− 779.77	**1623.46**	$\mu_l = \mu_0 + \mu_1 I + \mu_2 T, \sigma$
Barcaldine post office	Stationary	− 733.20	1505.18	μ, σ
	Time	− 721.59	1498.50	$\mu_l = \mu_0 + \mu_1 T, \sigma$
	CD	− 635.98	**1344.19**	$\mu_l = \mu_0 + \mu_1 E + \mu_2 E^2$
				$\sigma_l = \sigma_0 + \sigma_1 E + \sigma_2 E^2$
	Time + CD	− 628.05	1353.58	$\mu_l = \mu_0 + \mu_1 E + \mu_2 E^2 + \mu_3 T + \mu_4 T^2$
				$\sigma_l = \sigma_0 + \sigma_1 E + \sigma_2 T$
Ceduna AMO	Stationary	− 934.32	1898.72	μ, σ
	Time	− 924.77	1890.45	$\mu_l = \mu_0 + \mu_1 T, \sigma$
	CD	− 919.05	1888.54	$\mu_l = \mu_0 + \mu_1 I + \mu_2 I^2, \sigma$
	***Time* + CD**	− 892.92	**1861.80**	$\mu_l = \mu_0 + \mu_1 I + \mu_2 I^2 + \mu_3 T + \mu_4 T^2$
				$\sigma_l = \sigma_0 + \sigma_1 I + \sigma_2 T$

Table 3 (continued)

Station	Model	l_{ind}	CL-AIC	Model parameters
Adelaide airport	Stationary	− 885.62	1803.53	μ, σ
	Time	− 867.75	1790.75	$\mu_l = \mu_0 + \mu_1 T + \mu_2 T^2, \sigma$
	CD	− 884.90	1810.97	$\mu, \sigma_l = \sigma_0 + \sigma_1 I$
	Time + CD	− 842.22	**1750.65**	$\mu_l = \mu_0 + \mu_1 I + \mu_2 T + \mu_3 T^2$
				$\sigma_l = \sigma_0 + \sigma_1 I + \sigma_2 T$
Laverton RAAF	Stationary	− 939.13	1908.59	μ, σ
	Time	− 931.24	**1902.91**	$\mu_l = \mu_0 + \mu_1 T, \sigma$
	CD	− 932.31	1904.82	$\mu, \sigma_l = \sigma_0 + \sigma_1 I + \sigma_2 I^2$
	Time + CD	− 922.50	1905.08	$\mu_l = \mu_0 + \mu_1 I + \mu_2 I^2 + \mu_3 T, \sigma$
Walpeup research	Stationary	− 915.68	1866.35	μ, σ
	Time	− 864.87	1788.51	$\mu_l = \mu_0 + \mu_1 T + \mu_2 T^2, \sigma$
	CD	− 908.46	1865.52	$\mu_l = \mu_0 + \mu_1 I, \sigma$
	Time + CD	− 846.70	**1772.17**	$\mu_l = \mu_0 + \mu_1 I + \mu_2 T + \mu_3 T^2$
				$\sigma_l = \sigma_0 + \sigma_1 I + \sigma_2 T$

Bold font indicates the best model having the lowest CL-AIC value

* κ, θ, η are constant for all models

T = Time, E = ENSO, I = IOD, S = SAM

AMT during the study period (Figure S8 in the supplementary section).

In general, for all the stations, the difference between the stationary and non-stationary models incorporating the CDs as covariates decreased with the return period, as shown in the supplementary section (Figures S9–S13). Also, the stations where IOD was selected as the CD showed a significant difference between stationary and non-stationary models compared to the other stations where ENSO and SAM were selected as the CDs.

The average difference between the stationary model and the non-stationary models considering the CD alone as covariate ranged from − 3.0 to 1.5 °C (+ CD) and − 0.6 to 3.4 °C (– CD). In contrast, this difference became − 1.9 to 2.2 °C ("*Time* + CD") and − 1.6 to 4.7 °C ("*Time*–CD") in the case of the combination of two covariates—*Time* and selected CD.

Although *Time* had the overall dominance as a covariate on the computed quantiles for all the return periods compared to the selected climate indices, different covariates or combinations of them yielded the maximum quantiles for different return periods and stations. It should be noted that non-stationary TDF curves should be adopted in practice irrespective of its difference with the stationary TDF curves.

5 Conclusion

In this study, the formulation of stationary and non-stationary TDF curves was based on temperature time series from 82 weather stations located in Australia using the GEV distribution. Initially, the augmented Dickey-Fuller (ADF) test was conducted to identify non-stationarity in temperature time series and non-stationarity was found to be present in the data series.

The long-range relationships between the seasonal CDs (ENSO, IOD and SAM) and temperature data from 1969 to 2021 were investigated using the Pearson correlation coefficient to find out the best covariates in non-stationary TDF models. The magnitude of correlation coefficients of ENSO increases towards the east of Australia, and these coefficients are significant during SON and DJF seasons. The AMT observed at stations in the southeastern region of Australia, especially in the inland and coastal region of Victoria and South Australia, showed a significant correlation with IOD during SON. SAM showed a strong correlation with the annual temperature at the stations located in the coastal regions of Western Australia.

Stationary TDF curves showed an increase and decrease in design temperatures with higher return periods and an increase in duration, respectively. In the case of non-stationary TDF models, the location and scale parameters were modelled as being dependent on time and climate indicators for the selected stations. Inclusion of the selected covariates in non-stationary TDF models enhanced goodness-of-fit compared to the stationary TDF model for the corresponding station. Similar results were found by Ouarda and Charron (2018) where the influence of the climate oscillation pattern was found to be more prominent than the temporal trend. Furthermore, the best goodness-of-fit of the TDF model based on the AIC values was obtained with a combination of both covariates *Time* and selected
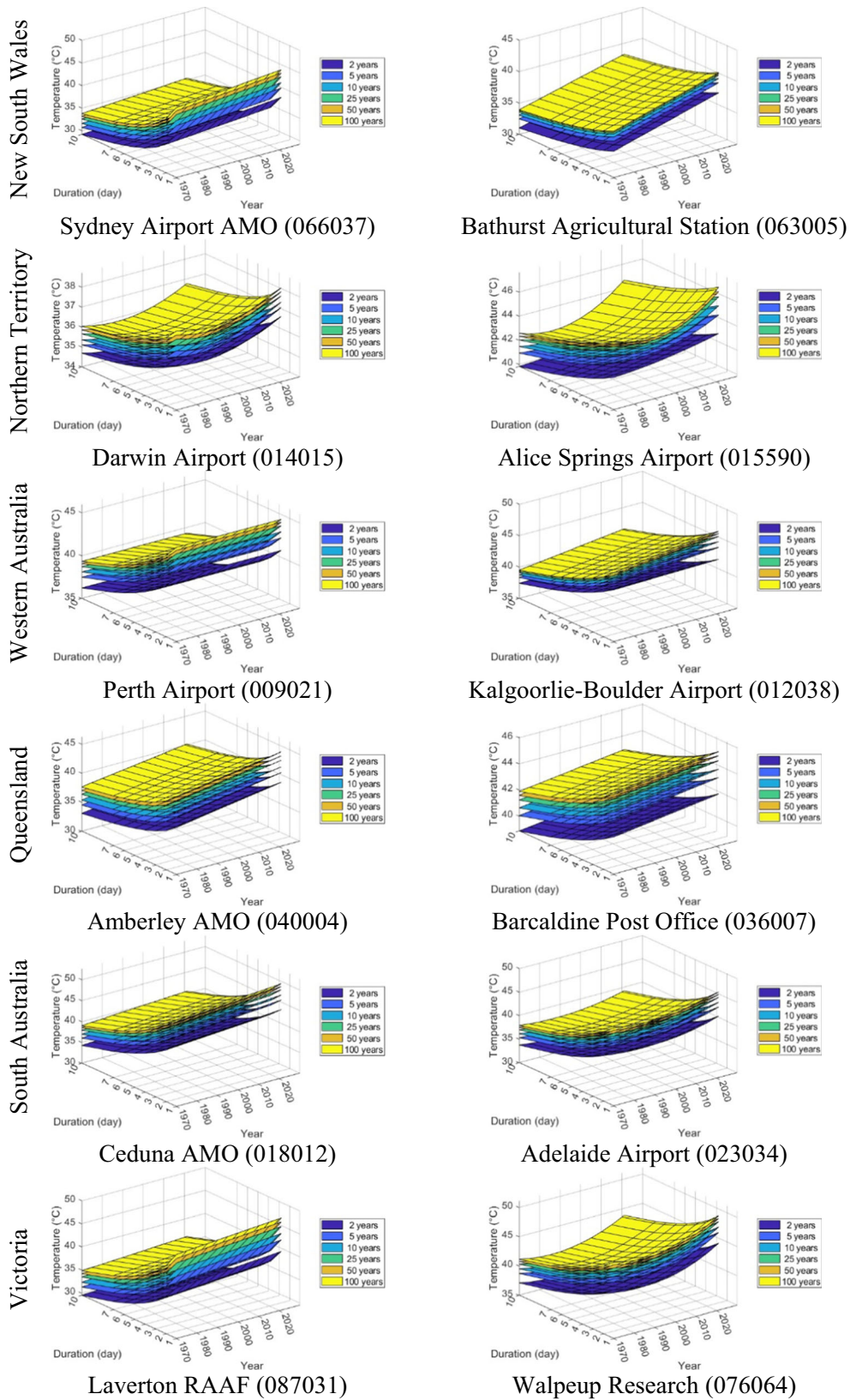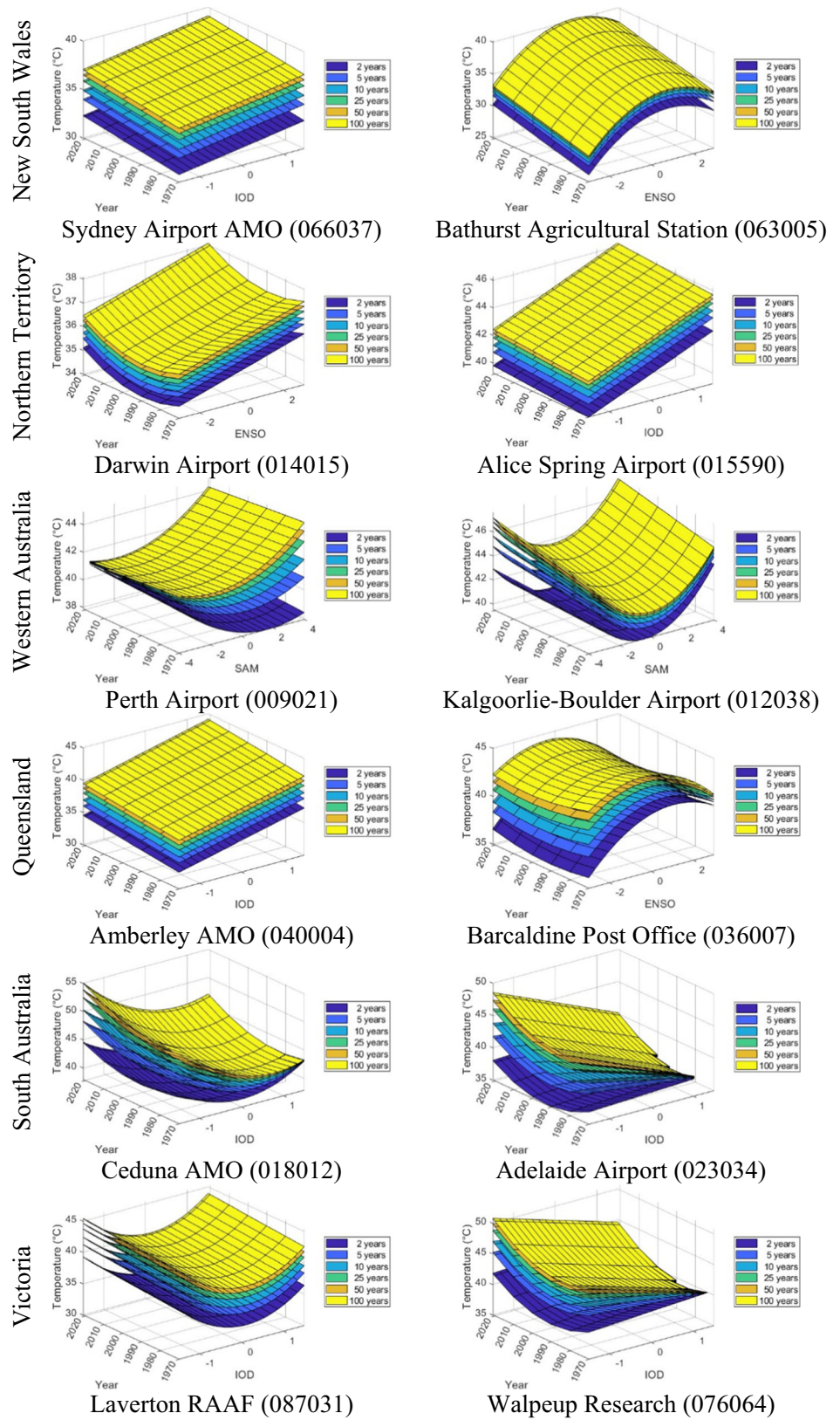
Fig. 5 Non-stationary TDF surfaces with *Time* covariates for 2, 5, 10, 25, 50 and 100 years return periods
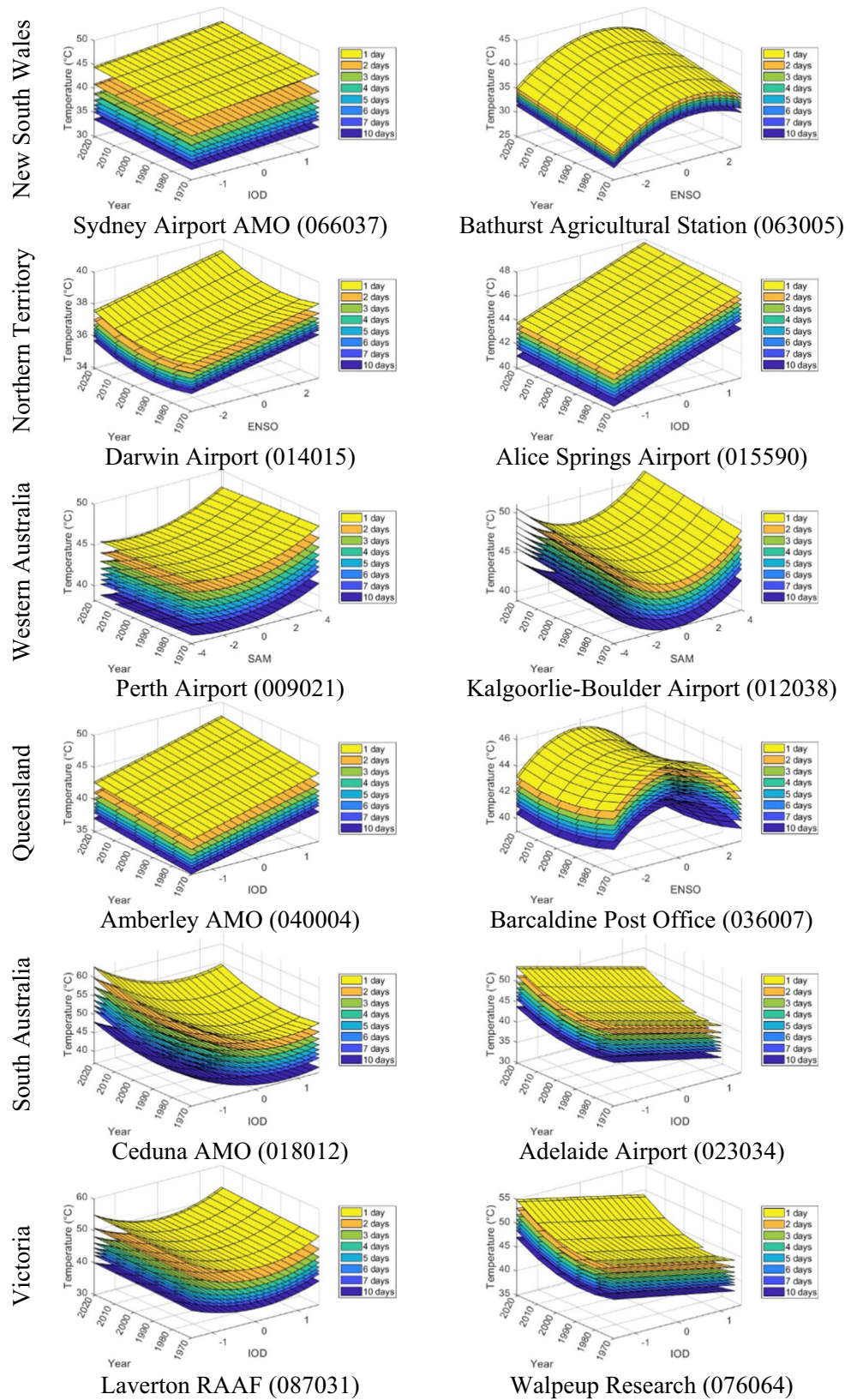
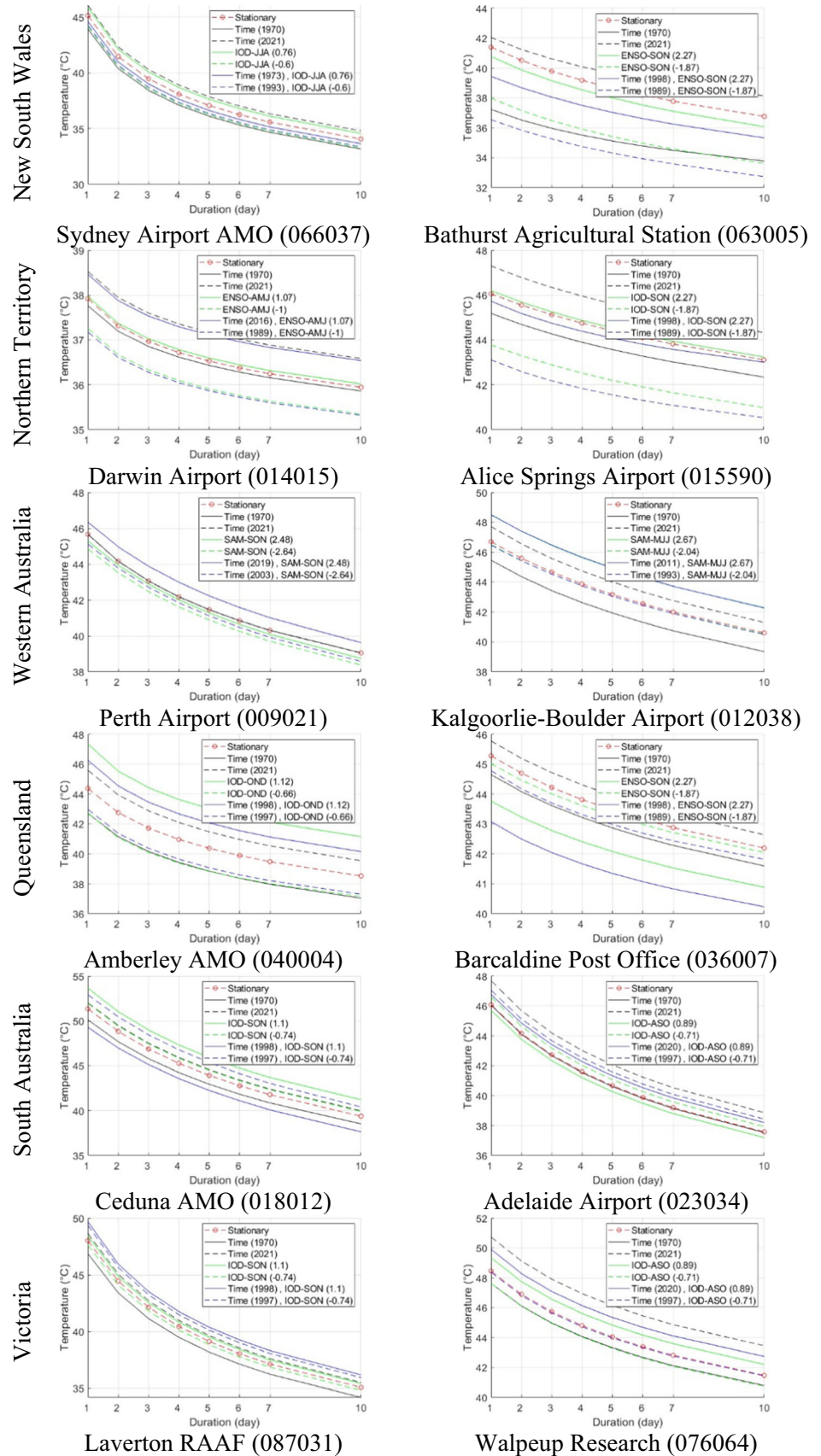Fig. 6 Non-stationary TDF surfaces with CD covariates for 2, 5, 10, 25, 50 and 100 years return periods
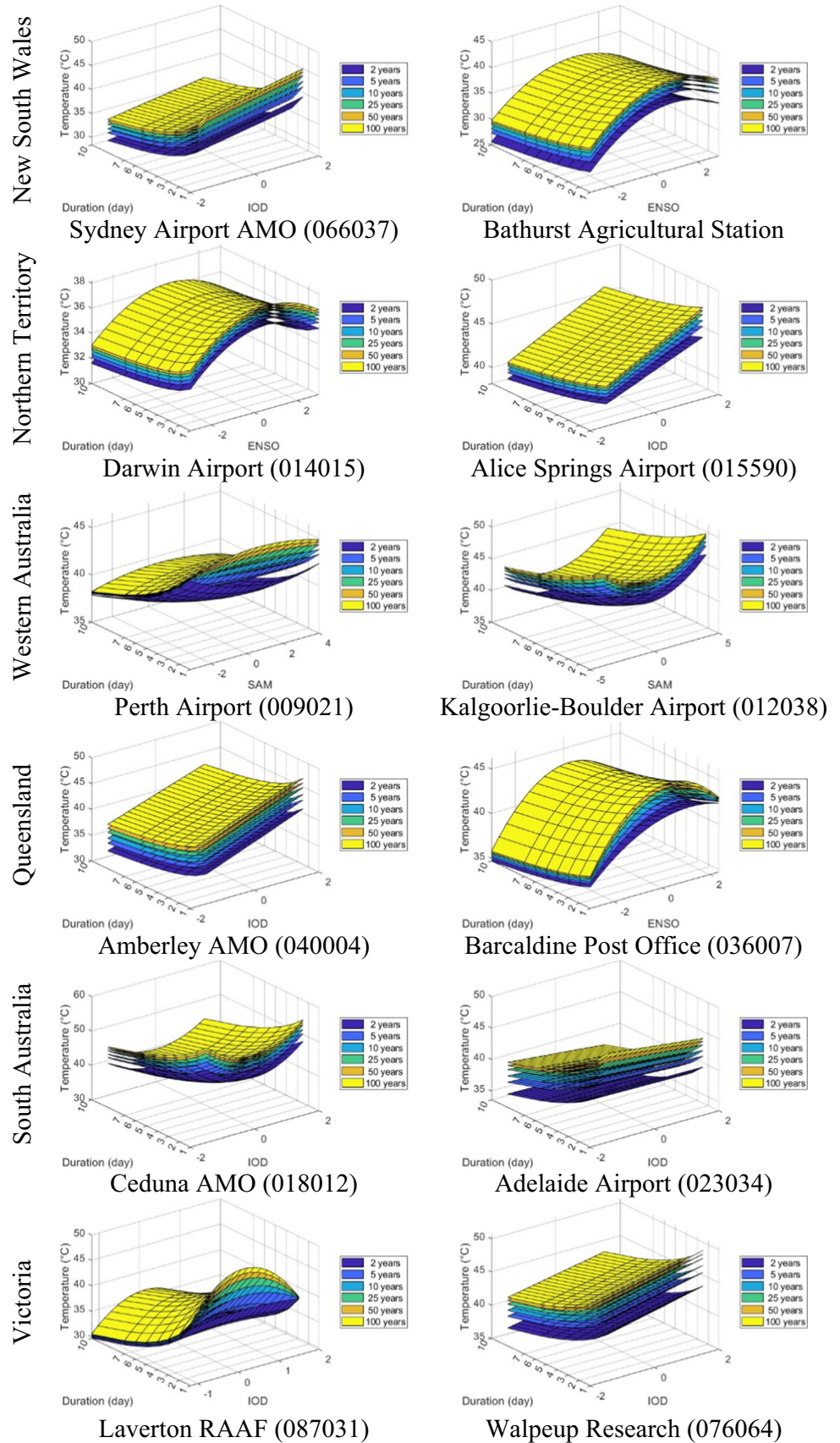
Fig. 7 Non-stationary TDF surfaces with *Time* and CD as covariates of 5-days duration for 2, 5, 10, 25, 50 and 100 years return periods

Sydney Airport AMO (066037)

Bathurst Agricultural Station (063005)

Darwin Airport (014015)

Alice Spring Airport (015590)

Perth Airport (009021)

Kalgoorlie-Boulder Airport (012038)

Amberley AMO (040004)

Barcaldine Post Office (036007)

Ceduna AMO (018012)

Adelaide Airport (023034)

Laverton RAAF (087031)

Walpeup Research (076064)

Fig. 8 Non-stationary TDF surfaces with *Time* and CD as covariates of 50-year return period for 1, 2, 3, 4, 5, 6, 7 and 10 days durations

Fig. 9 Comparison between stationary and non-stationary TDF curves (50-year quantiles)

New South Wales — Sydney Airport AMO (066037)

Bathurst Agricultural Station (063005)

Northern Territory — Darwin Airport (014015)

Alice Springs Airport (015590)

Western Australia — Perth Airport (009021)

Kalgoorlie-Boulder Airport (012038)

Queensland — Amberley AMO (040004)

Barcaldine Post Office (036007)

South Australia — Ceduna AMO (018012)

Adelaide Airport (023034)

Victoria — Laverton RAAF (087031)

Walpeup Research (076064)

CD for most of the stations. These results highlighted the importance of considering the combined effect of the temporal trend caused by global warming and CDs in statistical models used to predict design temperature.

The non-stationary quantiles computed with the first and last years of the study period and with the years of highest and lowest values of the selected seasonal CDs were compared with the stationary model to display the quantiles' temporal movement and the influence of the extreme conditions on the quantiles. In most cases, the stationary TDF model underestimated the design temperature compared to the non-stationary model, including *Time* as a covariate. This conveys a crucial message that the non-stationary framework for designing temperature facilities in Australia could be considered a stronger option than the traditional stationary approach. In addition, TDF curves developed in this study can be applied to a range of sectors such as agriculture, health care and energy production and can be a useful tool for policymakers and planners.

Data availability The data used in this study can be obtained by contacting the Australian Bureau of Meteorology (by paying a prescribed fee) (Australia's official weather forecasts & weather radar—Bureau of Meteorology (bom.gov.au)). Nino3.4 and DMI data used in this study can be obtained freely from NOAA (https://psl.noaa.gov/gcos_wgsp/Timeseries/Nino34/) and (https://psl.noaa.gov/gcos_wgsp/Time series /DMI/; and SAM data has been obtained from NERC (http://www.nerc-bas.ac.uk/ icd/gjma/sam.html).

Declarations

Competing interests The authors declare no competing interests.

References

Adlouni SE, Ouarda TBMJ (2009) Joint Bayesian model selection and parameter estimation of the generalized extreme value model with covariates using birth-death Markov chain Monte Carlo. Water Resour Res 45(6):1–11. https://doi.org/10.1029/2007WR006427

Arblaster JM, Alexander LV (2012) The impact of the El Nio-Southern oscillation on maximum temperature extremes. Geophys Res Lett 39(20):2–6. https://doi.org/10.1029/2012GL053409

Bellenger H et al (2014) ENSO representation in climate models: from CMIP3 to CMIP5. Clim Dyn 42(7–8):1999–2018. https://doi.org/10.1007/s00382-013-1783-z

Berghuijs WR et al (2019) Growing spatial scales of synchronous river flooding in Europe. Geophys Res Lett 46(3):1423–1428. https://doi.org/10.1029/2018GL081883

Boschat G et al (2015) Large scale and sub-regional connections in the lead up to summer heat wave and extreme rainfall events in eastern Australia. Clim Dyn 44(7–8):1823–1840. https://doi.org/10.1007/s00382-014-2214-5

Cai W, Van Rensch P (2012) The 2011 southeast Queensland extreme summer rainfall: a confirmation of a negative Pacific Decadal Oscillation phase? Geophys Res Lett 39(8):1–7. https://doi.org/10.1029/2011GL050820

Cai W, Cowan T, Raupach M (2009a) Positive Indian Ocean dipole events precondition southeast Australia bushfires. Geophys Res Lett. https://doi.org/10.1029/2009GL039902

Cai W, Cowan T, Sullivan A (2009b) Recent unprecedented skewness towards positive Indian Ocean Dipole occurrences and its impact on Australian rainfall. Geophys Res Lett 36(11):1–5. https://doi.org/10.1029/2009GL037604

Cai W et al (2011) Teleconnection pathways of ENSO and the IOD and the mechanisms for impacts on Australian rainfall. J Clim 24(15):3910–3923. https://doi.org/10.1175/2011JCLI4129.1

Cai W et al (2014) Increasing frequency of extreme El Niño events due to greenhouse warming. Nat Clim Chang 4(2):111–116. https://doi.org/10.1038/nclimate2100

Cheng L, Aghakouchak A (2014) Nonstationary precipitation intensity-duration-frequency curves for infrastructure design in a changing climate. Sci Rep 4:1–6. https://doi.org/10.1038/srep07093

Cheng L et al (2014) Non-stationary extreme value analysis in a changing climate. Clim Change 127(2):353–369. https://doi.org/10.1007/s10584-014-1254-5

Chowdary JS, John N, Gnanaseelan C (2014) Interannual variability of surface air-temperature over India: Impact of ENSO and Indian Ocean Sea surface temperature. Int J Climatol 34(2):416–429. https://doi.org/10.1002/joc.3695

Coles S (2001) An introduction to statistical modeling of extreme values. Springer

Cowan T et al (2014) More frequent, longer, and hotter heat waves for Australia in the Twenty-First Century. J Clim 27(15):5851–5871. https://doi.org/10.1175/JCLI-D-14-00092.1

CSIRO and Australian Government (Bureau of Meteorology) (2020) State of the Climate 2020: Australia's changing climate', Medicine, pp 1–24. Available at: https://apo.org.au/node/309418

Devi R, Gouda KC, Lenka S (2022) Temperature-duration-frequency analysis over Delhi and Bengaluru city in India. Theoret Appl

Climatol 147(1–2):291–305. https://doi.org/10.1007/s00704-021-03824-5

Galiatsatou P, Iliadis C (2022) Intensity-duration-frequency curves at ungauged sites in a changing climate for sustainable stormwater networks. Sustain Switz 14(3):1–24. https://doi.org/10.3390/su14031229

Ganguli P, Coulibaly P (2017) Does nonstationarity in rainfall require nonstationary intensity-duration-frequency curves? Hydrol Earth Syst Sci 21(12):6461–6483. https://doi.org/10.5194/hess-21-6461-2017

Guthrie M (2021) Climate drivers of the South West Land Division. Available at: https://www.agric.wa.gov.au/climate-weather/climate-drivers-south-west-land-division (Accessed: 9 June 2022)

Haddad K (2021) Selection of the best fit probability distributions for temperature data and the use of L-moment ratio diagram method: a case study for NSW in Australia. Theoret Appl Climatol 143(3–4):1261–1284. https://doi.org/10.1007/s00704-020-03455-2

Halpert MS, Ropelewski CF (1992) Surface temperature patterns associated with the southern oscillation. J Clim. https://doi.org/10.1175/1520-0442(1992)005%3c0577:stpawt%3e2.0.co;2

Hendon HH, Thompson DWJ, Wheeler MC (2007) Australian rainfall and surface temperature variations associated with the Southern Hemisphere annular mode. J Clim 20(11):2452–2467. https://doi.org/10.1175/JCLI4134.1

Hundecha Y et al (2008) A nonstationary extreme value analysis for the assessment of changes in extreme annual wind speed over the gulf of St. Lawrence Canada. J Appl Meteorol Climatol 47(11):2745–2759. https://doi.org/10.1175/2008JAMC1665.1

IPCC (2018) Summary for Policymakers. In: Global warming of 1.5 °C. An IPCC Special Report on the impacts of global warming of 1.5 °C above pre-industrial levels and related global greenhouse gas emission pathways, in the context of strengthening the global response to, World Meteorological Organization, Geneva, Switzerland. Geneva, Switzerland. doi: https://doi.org/10.1017/CBO9781107415324

Jakob D (2013) In: AghaKouchak A et al (eds) Nonstationarity in extremes and engineering design. Springer Netherlands, Dordrecht pp. 363–417. https://doi.org/10.1007/978-94-007-4479-0_13

Katz RW, Parlange MB, Naveau P (2002) Statistics of extremes in hydrology. Adv Water Resour 25(8–12):1287–1304. https://doi.org/10.1016/S0309-1708(02)00056-8

Koutsoyiannis D, Kozonis D, Manetas A (1998) A mathematical framework for studying rainfall intensity-duration-frequency relationships. J Hydrol 206(1–2):118–135. https://doi.org/10.1016/S0022-1694(98)00097-3

Kwon H-H, Lall U (2016) A copula-based nonstationary frequency analysis for the 2012–2015 drought in California. Water Resour Res 52(7):5662–5675. https://doi.org/10.1002/2016WR018959

Liu L et al (2014) Indian Ocean variability in the CMIP5 multi-model ensemble: The zonal dipole mode. Clim Dyn 43(5–6):1715–1730. https://doi.org/10.1007/s00382-013-2000-9

Lorenz R, Stalhandske Z, Fischer EM (2019) Detection of a climate change signal in extreme heat, heat stress, and cold in europe from observations. Geophys Res Lett 46(14):8363–8374. https://doi.org/10.1029/2019GL082062

Maher P, Sherwood SC (2014) Disentangling the multiple sources of large-scale variability in Australian wintertime precipitation. J Clim 27(17):6377–6392. https://doi.org/10.1175/JCLI-D-13-00659.1

Meyers G et al (2007) The years of El Niño, La Niña and interactions with the tropical Indian Ocean. J Clim 20(13):2872–2880. https://doi.org/10.1175/JCLI4152.1

Min SK, Cai W, Whetton P (2013) Influence of climate variability on seasonal extremes over Australia. J Geophys Res Atmos 118(2):643–654. https://doi.org/10.1002/jgrd.50164

Nicholls N (1985) Towards the prediction of major Australian droughts. Aust Meteorol Mag 33:161–166

Nicholls N, Lucas C (2007) Interannual variations of area burnt in Tasmanian bushfires: relationships with climate and predictability. Int J Wildland Fire 16(5):540–546. https://doi.org/10.1071/WF06125

Oliveira FNM, Ambrizzi T (2017) The effects of ENSO-types and SAM on the large-scale southern blockings. Int J Climatol 37(7):3067–3081. https://doi.org/10.1002/joc.4899

Omer A et al (2020) 'Natural and anthropogenic influences on the recent droughts in yellow river basin China. Sci Total Environ. https://doi.org/10.1016/j.scitotenv.2019.135428

Ouarda TBMJ, Charron C (2018) Nonstationary temperature-duration-frequency curves. Sci Rep 8(1):1–8. https://doi.org/10.1038/s41598-018-33974-y

Ouarda TBMJ, Yousef LA, Charron C (2019) Non-stationary intensity-duration-frequency curves integrating information concerning teleconnections and climate change. Int J Climatol 39(4):2306–2323. https://doi.org/10.1002/joc.5953

Ouarda TBMJ, Charron C, St-Hilaire A (2020) Uncertainty of stationary and nonstationary models for rainfall frequency analysis. Int J Climatol 40(4):2373–2392. https://doi.org/10.1002/joc.6339

Parker TJ, Berry GJ, Reeder MJ (2013) The influence of tropical cyclones on heat waves in Southeastern Australia. Geophys Res Lett 40(23):6264–6270. https://doi.org/10.1002/2013GL058257

Perkins SE, Argüeso D, White CJ (2015) Relationships between climate variability, soil moisture, and Australian heatwaves. J Geophys Res Atmos 120(16):8144–8164. https://doi.org/10.1002/2015JD023592

Power S et al (1999) Inter-decadal modulation of the impact of ENSO on Australia. Clim Dyn 15(5):319–324. https://doi.org/10.1007/s003820050284

Power SB et al (2006) The predictability of interdecadal changes in ENSO activity and ENSO teleconnections. J Clim 19(19):4755–4771

Risbey JS et al (2009) On the remote drivers of rainfall variability in Australia. Mon Weather Rev 137(10):3233–3253. https://doi.org/10.1175/2009MWR2861.1

Ropelewski CF, Halpert MS (1988) Precipitation patterns associated with the high index phase of the southern oscillation. J Clim 2(3):268–284

Rossi F, Villani P (1994) A project for regional analysis of floods in Italy, in Rossi, G., Harmancio\uglu, N., and Yevjevich, V. (eds) Coping with Floods. Dordrecht: Springer Netherlands, pp 193–217. https://doi.org/10.1007/978-94-011-1098-3_11

Saji NH et al (1999) A dipole mode in the tropical Indian ocean. Nature 401(6751):360–363. https://doi.org/10.1038/43854

Sarhadi A, Soulis ED (2017) Time-varying extreme rainfall intensity-duration-frequency curves in a changing climate. Geophys Res Lett 44(5):2454–2463. https://doi.org/10.1002/2016GL072201

Sein KK, Chidthaisong A, Oo KL (2018) Observed trends and changes in temperature and precipitation extreme indices over Myanmar. Atmosphere 9(12):477

Singh VP, Zhang L (2007) IDF Curves Using the Frank Archimedean Copula. J Hydrol Eng 12(6):651–662. https://doi.org/10.1061/(ASCE)1084-0699(2007)12:6(651).

Spinoni J, Naumann G, Vogt JV (2017) Pan-European seasonal trends and recent changes of drought frequency and severity. Global Planet Change 148:113–130. https://doi.org/10.1016/j.gloplacha.2016.11.013

Sugahara S, da Rocha RP, Silveira R (2009) Non-stationary frequency analysis of extreme daily rainfall in Sao Paulo, Brazil. Int J Climatol 29(9):1339–1349. https://doi.org/10.1002/joc.1760

Suman M, Maity R (2020) Southward shift of precipitation extremes over south Asia: Evidences from CORDEX data. Sci Rep 10(1):1–11. https://doi.org/10.1038/s41598-020-63571-x

Thompson DW, Wallace JM, Hegerl GC (2000) Annular modes in the extratropical circulation Part II Trends. J Climate 13(5):1018–1036

Turney CSM et al (2007) Quaternary climatic, environmental and archaeological change in Australasia. J Quat Sci 22(5):421–422. https://doi.org/10.1002/jqs.1139

Ummenhofer CC et al (2009) What causes southeast Australia's worst droughts? Geophys Res Lett 36(4):1–6. https://doi.org/10.1029/2008GL036801

Ummenhofer CC et al (2011) Indian and Pacific Ocean influences on southeast Australian drought and soil moisture. J Clim 24(5):1313–1336. https://doi.org/10.1175/2010JCLI3475.1

Wang XL et al (2013) Historical changes in Australian temperature extremes as inferred from extreme value distribution analysis. Geophys Res Lett 40(3):573–578. https://doi.org/10.1002/grl.50132

White CJ et al (2013) On regional dynamical downscaling for the assessment and projection of temperature and precipitation extremes across Tasmania, Australia. Clim Dyn 41(11–12):3145–3165. https://doi.org/10.1007/s00382-013-1718-8

Yan H et al (2019) Next-generation intensity–duration–frequency curves to reduce errors in peak flood design. J Hydrol Eng 24(7):04019020. https://doi.org/10.1061/(asce)he.1943-5584.0001799

Yan H et al (2020) Evaluating next-generation intensity–duration–frequency curves for design flood estimates in the snow-dominated western United States. Hydrol Process 34(5):1255–1268. https://doi.org/10.1002/hyp.13673

Yilmaz AG, Perera BJC (2014) Extreme Rainfall Nonstationarity Investigation and Intensity–Frequency–Duration Relationship. J Hydrol Eng 19(6):1160–1172. https://doi.org/10.1061/(asce)he.1943-5584.0000878